New methodology of backbone curve for RC perforated shear walls

Jing-Shyang Yang[†]

Carson K.C. Mok Consulting Engineer, P.A., 9001 Ottawa Place, Silver Spring, MD 20910, U.S.A.

Franklin Y. Cheng[‡]

Department of Civil Engineering, University of Missouri-Rolla, Rolla, MO 65409, U.S.A.

Abstract. Following a series of experiments on isolated low-rise RC shear walls with openings, a theoretical study on the backbone curve of a perforated shear wall shows that there are some important observations from experimental results that make clear a semi-empirical formula of the backbone curve of a perforated wall. Critical shear zones can be depicted from the configuration of shear walls with openings. Different factors, including the size and location of shear wall openings, the wall's height/width ratio, horizontal and vertical steel bar ratios, and location and amount of diagonal steel bars are involved in the derivation of the backbone curve. Bending and shear effects are also considered in the paper. In addition, a comparison of load and displacement for solid and perforated shear walls is discussed. Generally, the comparison between experimental curves and computed backbone curves is favorable.

Key words: backbone curve; low-rise; shear wall; RC wall; perforated shear wall; load-displacement curve.

1. Introduction

Previous research focused for years on low-rise RC shear walls. Among them, Yamada *et al.* performed a series of static tests on RC shear walls with openings under monotonic loads. Test observations indicated that the thickness of walls and surrounding reinforcements of openings played an important role in the fracture modes. Analytically, the deformation of both the shear compressive resisting element and the flexural resisting element were introduced in the formation of the load-displacement relationship. The maximum strength of shear walls was formulated in this regard, which included reduction consideration of the size and shape of openings (Yamada *et al.* 1974).

Chiba *et al.* conducted a series of tests, including solid and perforated shear walls, and employed reinforcements, shear span length ratio, and axial stress as parameters in the study. For RC shear walls with openings, the size, number, location, and shape of the openings were also considered in

---

† Structural Engineer
‡ Curators' Professor Emeritus

the tests, during which the equations of maximum strength of walls were formed in the analytical study. Thus, a set of equations was derived. In addition, the reduction factors caused by the size and shape of openings were included as well (Chiba *et al*. 1985).

Sato *et al*. performed a set of tests in which specimens with a wall height/width ratio of 0.2 were used. Factors for sizes, locations, and number of openings were considered. Reinforcing methods around the openings for evaluation of the maximum shear strength and displacement of a shear wall were also considered. The equation for maximum shear strength of the shear wall was established in their study (Sato *et al.* 1987). Another study that focused on a number of small openings for pipes and ducts in shear walls was conducted by Sotomura *et al*. Web-reinforcements, size and location of openings, diagonal reinforcements between openings, axial forces, and vertical reinforcement distribution on both sides of the wall were of main concern. The results showed the proposed equation for the ultimate load of a shear wall is the summation of the ultimate strength of all independent walls. The independent wall applied here means the portion of the wall between openings (Sotomura *et al*. 1985).

In general, the aforementioned studies show some evidence from the experimental work. First, the openings trigger the initial cracks and its corresponding reduction of a wall's strength. Second, the location of openings may develop two possible failure patterns, sliding shear failure or diagonal compression failure. Also, Sato (Sato *et al*. 1987) and Chiba (Chiba *et al*. 1985) proposed shear span length ratios, while Sotomura (Sotomura *et al*. 1985) considered the concept of the effective area of a wall as well as dowel action, in the formation of the ultimate load of a shear wall. The studies above were concerned about low-rise RC shear walls, either solid or perforated, with boundary columns and a beam on the top of a wall. In addition, a wall's maximum strength was proposed for evaluation of a shear wall.

Cheng and Mertz conducted an analytical study (Cheng and Mertz 1989, 1993) in which the experimental work was performed under Sheu at National Cheng Kung University (NCKU) in Taiwan (Sheu 1988). This study involved the low-rise RC solid shear walls without boundary columns, and without a concrete beam on the top, which reflects many cases in nuclear power plants and buildings requiring higher construction standards. Through their study, for a crucial role of shear effect in RC shear walls, the total load-displacement relationship of a shear wall was developed and was composed of shear and bending load-displacement curves. At these backbone curves, i.e., load-displacement curves, elastic, cracking, yielding, and failure stages were clearly defined. Theoretical derivations also showed the relationship between moment, shear, shear strain, and curvature. This paper studies the continued work, which focuses on low-rise RC perforated shear walls without boundary columns and without a concrete beam on the top of a wall. Single windows, double windows, doors, and single slits were considered in this study. Some solid walls were also tested in order to discriminate between solid and perforated shear walls.

2. Test specimens and schedule

Experimental work in this cooperative research was also conducted under Sheu at NCKU (Sheu 1988). Test specimens were squat RC shear walls with openings, or perforated shear walls; there were no concrete columns and beams around the walls. Test apparatus shown in Fig. 1 has a large frame fixed at ground level for a stable test environment. Specimens are embedded in the steel beam on the ground. Lateral force is transferred to the specimen by attaching a steel beam to the top of
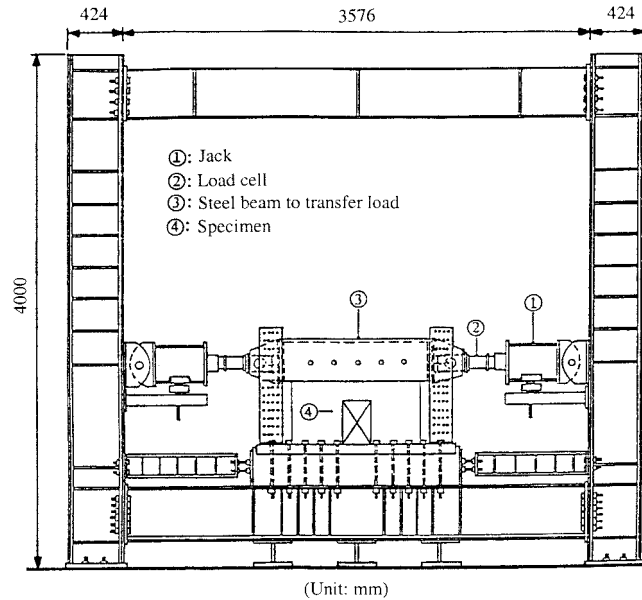
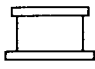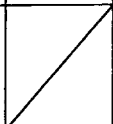(Unit: mm)
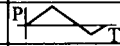
Fig. 1 Experimental apparatus for shear walls
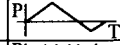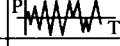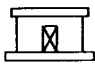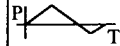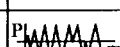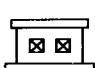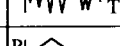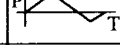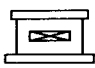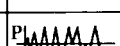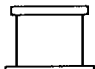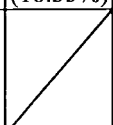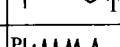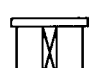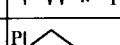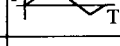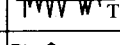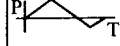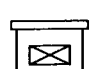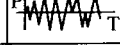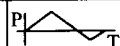
the wall. The force system is composed of two jacks set up on both sides of the specimen. The top of the specimen is allowed to move or rotate.

Table 1 shows a summary of the test schedule. There are two kinds of loading patterns applied to each type of specimen; these are both single cyclic (monotonic) loading and quasi-seismic type loading. Two groups of shear walls were studied in this program in which solid and perforated shear walls were examined in each group. Group I, with a height/width ratio of 0.5 (100 cm × 50 cm × 10 cm), has yielding strength of 4617 Kg/cm² for steel bars. Group II, with a height/width ratio of 0.75 (100 cm × 75 cm × 10 cm), has yielding strength of 5005 Kg/cm² for steel bars. The compressive strength of concrete in this study ranges from 254 to 345 Kg/cm². The opening rate for shear walls in Group I was 16.35%, but 21.8% in Group II. Diagonal bars were only used for perforated shear walls.

Fig. 2 shows the arrangement of steel bars in a specimen for a shear wall (SWO-5E, 6E) with double windows. Diagonal bars were laid around the corners of openings in order to strengthen them. Locations of load cells for specimens are shown in Fig. 1. Potential meters and dial gauges were applied to measure displacements in the horizontal direction, while clip-on gauges were employed for vertical displacements.

A computer-controlled force system adequately discriminates between two different control stages during load process, either under a cyclic loading or an earthquake type loading. For the case of a cyclic loading, the first loading stage was controlled at a load increment of 0.5-1 tons up to the yielding point of a shear wall. After yielding of the wall, displacement control with an increment of 0.5-1 mm dominates the rest of the test to prevent extensive cracks in a specimen. For earthquake type loading, the first three cycles were controlled by the load increment, and subsequently, controlled by the displacement increment.

Table 1 Summary of test specimen and schedule

Group ($\frac{L}{W}$)	Type	Specimen No.	Specimen sketch	Wall size WxLxt (cm)	Opening size $N \times L_o \times W_o$	(Steel bar) Vertical Horizontal Diagonal	$f_y \left(\frac{kg}{cm^2}\right)$	$f_c' \left(\frac{kg}{cm^2}\right)$	$f_{sp}' \left(\frac{kg}{cm^2}\right)$	Loading history
Group I ($\frac{1}{2}$)	W/o opening	SW-0E				10-D10		254	25.0	
		SW-1E				5-D10		345	24.7	
		SW-2E				—		268	25.7	
	Single door	SWO-3E		100 x 50 x 10	$1 \times 21.8 \times *2\ 37.5\ (16.35\%)$	10-D10 / 5-D10	5005	299	22.6	
		SWO-4E				*1 D-D13		316	17.0	
	Double window	SWO-5E			$2 \times 21.8 \times 18.75\ (16.35\%)$	10-D10 / 5-D10		329	31.1	
		SWO-6E				D-D13		329	31.0	
	Single window	SWO-7E			$1 \times 65.4 \times 12.5\ (16.35\%)$	10-D10 / 5-D10		328	24.0	
		SWO-8E				D-D13		328	24.0	
Group II ($\frac{3}{4}$)	W/o opening	SW-9E				10-D13 / 7-D13		294	25.7	
		SW-10E				—		312	25.7	
	Single slit	SWO-11E		100 x 75 x 10	$1 \times 21.8 \times 75.0\ (21.8\%)$	8-D13 / 7-D13	4617	297	22.5	
		SWO-12E				D-D13		297	22.5	
	Double window	SWO-13E			$2 \times 21.8 \times 37.5\ (21.8\%)$	10-D13 / 7-D13		321	23.2	
		SWO-14E				D-D13		325	23.6	
	Single window	SWO-15E			$1 \times 65.4 \times 25.0\ (21.8\%)$	10-D13 / 7-D13		279	20.7	
		SWO-16E				D-D13		283	19.8	

*1 Diagonal bar   *2 Opening rate

3. Test results and comparison

Characteristics of perforated shear walls are depicted in Fig. 3. Here the dotted smooth curve represents a schematic test result at different loading stages. The solid curve (i.e., the simplified curve), composed of four straight lines, indicates the defined load-displacement relationship (or backbone curve). In this figure, four critical loading points describe the mechanical properties of a shear wall at four different stages in which this project follows analytically.

Cracking point (C) denotes the loading point where initial cracks first appear. Yielding point (Y)

Double window (SWO-5E, 6E) (Unit: cm)
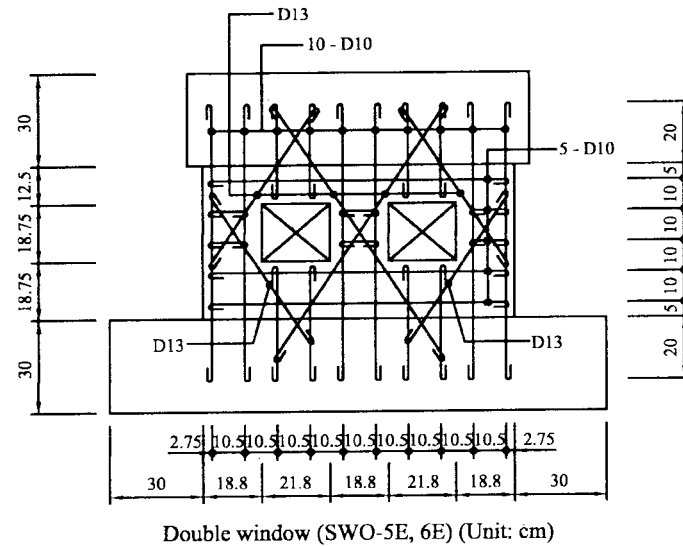
Fig. 2 Configuration of steel bars for shear walls
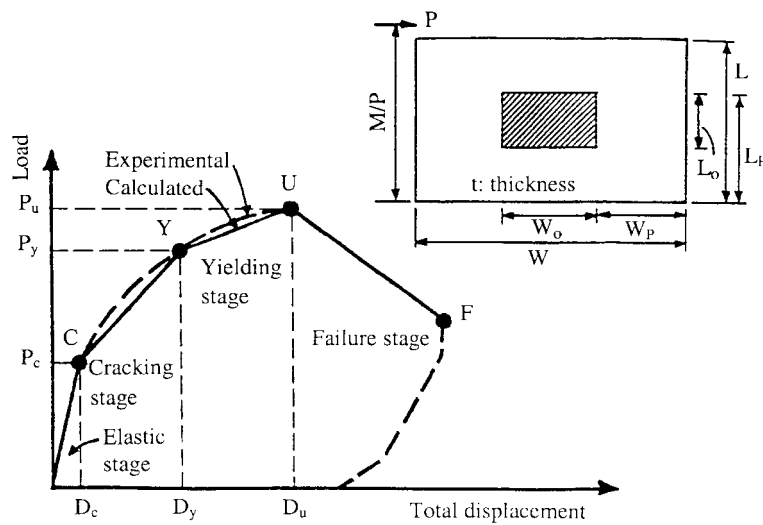
Fig. 3 Schematic diagram and defined backbone curve for perforated shear wall

occurs when the outermost steel bars reach yielding stress. When the applied lateral load can not be increased, ultimate point (U) is presented. After this culminating load point, the curve degrades. The curve goes downward until failure reference point (F). Four characteristic stages for a low-rise RC shear wall are then defined, including elastic, cracking, yielding, and failure.

From the test results, it can be seen that the cracking load for both solid and perforated shear walls is stable and ranges from 4 to 6 tons with an average of 4.8 tons. Solid shear walls have a higher yielding load, from 27 to 28 tons, than perforated shear walls, which ranges from 12 to 22 tons with a height/width ratio of 0.5, and from 7 to 18 tons with a height/width ratio of 0.75. The yielding load for solid shear walls is 27.65 tons on average. The average yielding load for all

perforated shear walls is 15.43 tons, about 56% of that for solid shear walls. Solid shear walls have stable ultimate loads, ranging from 32 to 34 tons with an average of 33.13 tons. Perforated shear walls have an average ultimate load of 21.22 tons (ranging from 16 to 25 tons), with a height/width ratio of 0.5; and an average of 14.87 tons (ranging from 9 to 20 tons), with a height/width ratio of 0.75. The overall average ultimate load ratio between perforated (18.04 tons) and solid (33.13 tons) is 0.54, about the same ratio as for the average yielding load for all perforated shear walls.

Displacement at the cracking point has a range of 0.2-0.7 mm for either solid or perforated shear walls. Solid shear walls, with a range of 2.6-3.7 mm, have an average yielding displacement of 3.35 mm. Average yielding displacements, for perforated shear walls of 2.1 mm and 2.2 mm for Group I and II respectively is about two thirds that of solid shear walls. These figures exclude the wall with a single slit (SWO-11E). Regarding ultimate displacement, an average of 3.79 mm for perforated shear walls is about two-fifths that of solid shear walls, an average of 9.62 mm.

The above observation indicates that openings in shear walls is a crucial factor in affecting load capacities and corresponding displacements of RC walls. In general, openings in a shear wall not only reduce load capacity at yielding and ultimate stages by an average of 50%, but also reduce maximum displacement by an average of 60%.

4. Curvature distribution

An analytical study shows that curvature starts from zero at the top of the wall, increases proportionally with square of depth, and reaches its highest value at the bottom of the wall (Cheng and Mertz 1989). Typical curvature distributions for solid and perforated shear walls, Fig. 4 and Fig. 5, respectively, show consistent phenomena with analytical derivation. For a shear wall, it is obvious that corresponding bending moment distributes from zero at the top to the maximum value at the bottom of the wall. Therefore, the curvature physically reflects the effect of flexural behavior on shear walls. From Fig. 4 and Fig. 5, due to relatively smaller bending effects on the top portion of a wall, the mechanical behavior may be near or within the elastic range. While a large bending moment prevails on the bottom portion of a wall, the wall's behavior shows highly inelastic
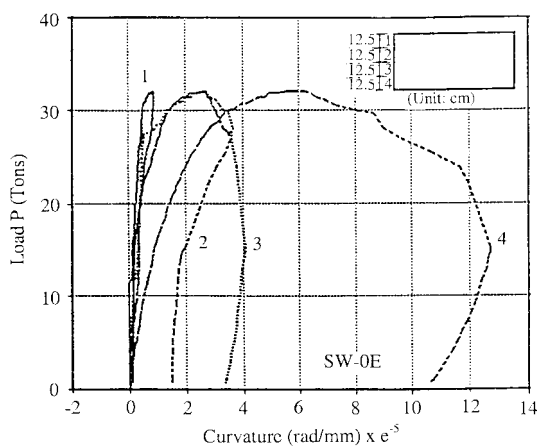

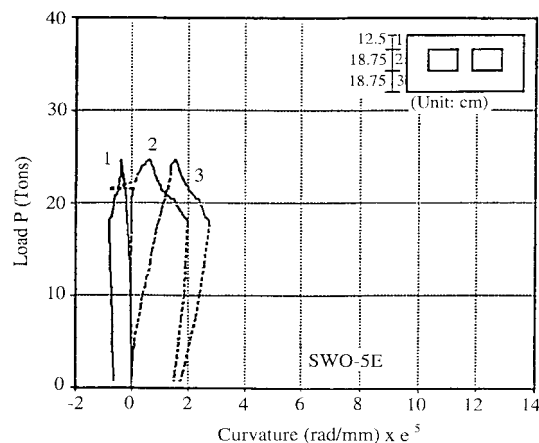Fig. 4 Load vs. curvature relationship for shear wall

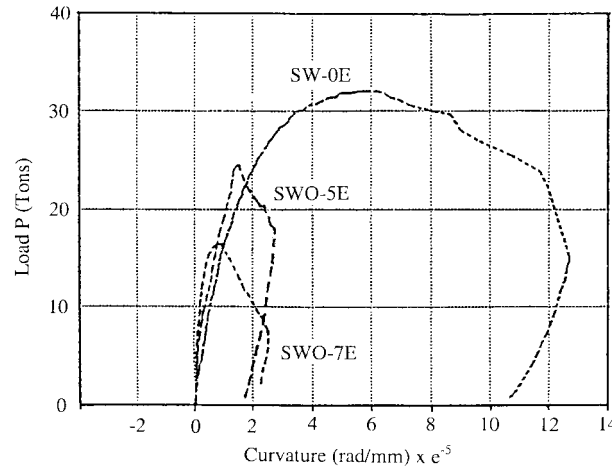Fig. 5 Load vs. curvature relationship for shear wall

Fig. 6 Load vs. curvature relationship at bottom portion of shear walls

behavior, i.e., a combination of nonlinear effects of both concrete and steel bars. In view of flexural behavior, either for a solid or perforated shear wall, the bottom portion of a RC shear wall contributes most to the load-displacement relationship of a shear wall. For the shear wall with double windows, the curvature reveals opposite rotation at the top segment of the wall. The possibilities of this reverse rotation phenomenon may be caused by several reasons, mainly by a small flexural moment induced in this portion and the development of initial diagonal cracks.

Fig. 6 shows the curvature distribution for the bottom portion of one solid and two perforated shear walls. Note that the perforated shear walls provide smaller curvature capacities. Thus, the openings in a wall restrict the process of flexural action.

5. Bending, shear and total load-displacement relationship

Backbone curve, or total load-displacement curve, of a shear wall is the combination of bending and shear load-displacement curves. The bending load-displacement curve is mainly related to the action of vertical steel bars, which can reflect flexural behavior of a wall. The shear load-displacement curve considers the behavior caused by the horizontal steel bars. In addition, concrete is another important resistant factor against the external force.

Based on Cheng-Mertz's study (Cheng and Mertz 1989) on low-rise RC solid shear wall, an average of 50% of total ultimate displacement is caused by a bending effect. Shear effect has almost the equivalent action of a bending effect. In this paper, Cheng and Mertz's approach was employed to calculate bending and shear displacements. It was found that bending displacement occupied about 13-40% of total lateral displacement for solid walls, while approximately 10%, and 10-45% of total displacement, was revealed by bending effects for Group I and II of perforated shear walls, respectively. Therefore, shear displacement, accounting for a high contribution of total lateral displacement, plays an important role in resisting force when a wall is subjected to an applied lateral load.

Next, compare bending as well as shear load-displacement relationships between perforated shear

walls with double windows SWO-5E (height/width ratio of 0.5) and SWO-11E (height/width ratio of 0.75). It is depicted that bending effects occupy a higher percentage of the total displacement for the wall with a height/width ratio of 0.75, than that for the wall with a height/width ratio of 0.5. The possible reason is that a low-rise RC shear wall with a higher height/width ratio may provide a larger bending effect in the blocks on the sides of, and between openings; the walls with a higher height/width ratio have larger longitudinal steel bars in shear walls.

Failure ductility is defined as the ratio of failure displacement to yielding displacement. It provides important information to reveal failure mechanism of both shear walls and the entire structure. Observations from the above experimental load-displacement relationships, for low-rise perforated shear walls, support 4.0 as a favorable failure ductility of perforated shear walls. This value is the same as Cheng-Mertz's study for low-rise solid shear walls.

6. Establishment of backbone curve

When an external lateral load is applied to a RC shear wall, concrete and steel bars start to create stresses resisting the external force. As the applied load increases, and cracks in the concrete appear, the wall triggers it's decay in strength and initiates larger displacement. Further loading widens initial diagonal cracks, as well as initial horizontal tension cracks, and creates new cracks. The wall then shows more complicated behavior due to the combination of flexure and shear. For solid shear walls, many apparent diagonal cracks and spalling of concrete on the compression side occur throughout the entire wall. Perforated shear walls undergo cracks and concrete crushing, which are mainly limited on both sides of, and between openings. It is apparent that the existence of openings caused perforated shear walls to develop a higher frequency of cracks in small size in comparison with solid shear walls. Some important observations led to the formation of equations which will be explained below.

7. Initial diagonal cracks

As stated above, initial cracks force walls to experience a decrease in strength capacity and an increase in lateral displacement. These cracks are initiated at the very early stage, so that they may
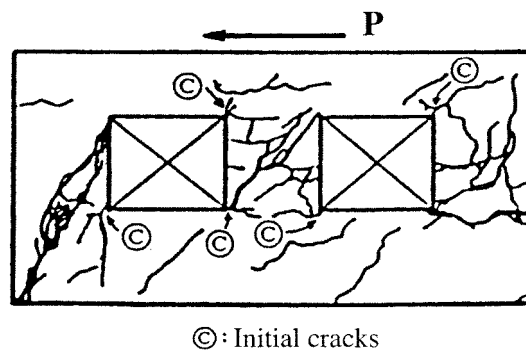

©：Initial cracks

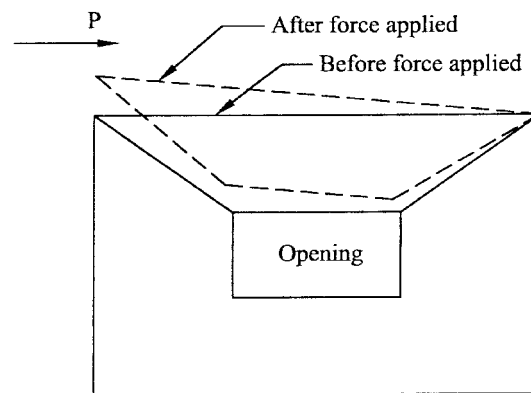Fig. 7 Crack development at failure stage for NCKU shear wall

Fig. 8 Cracking mechanism in top block of perforated shear wall

develop well in their width and length afterwards. Subsequent new and smaller cracks are mainly created around or within these initial cracks. Initial cracks may include diagonal cracks around the openings and horizontal tensile cracks at lower portions of the wall on the tension side. Initial diagonal cracks may start at the corners of openings either on tension or compression side (shown in Fig. 7). Those on the tension side usually occur first, since cracks are initiated by concrete, which has less tensile strength than its compressive strength, and also less than the yielding strength of steel bars. Diagonal cracks at the corners of openings are due to stress concentration, caused by both flexure and shear.

The aforementioned crack patterns for perforated shear walls develop a different mechanism from solid shear walls. One is the development of a wedge-shaped region. The other is the formation of a restricted hinge region (i.e., critical shear zone). The wedge-shaped region (Fig. 8) is formed when initial diagonal cracks separate a block on top from the rest of the shear wall at the early stage of loading history. This top block, showing negative curvature distribution as shown in Fig. 5, is regarded as near-elastic; and thus, vertical steel bars above the openings within this top block can be negligible. Therefore, vertical bars are only considered on both sides of the openings along the overall height of the wall regarding the load-displacement relationship.

According to Cheng and Mertz (Cheng *et al*. 1989, 1993), the hinging region is the solid RC shear wall itself. This region occurs where the coupled bending and shear actions exist. In this region, many major diagonal cracks are well formed and subsequent small cracks are woven together. Complicated coupling action due to bending and shear in this region allows the shear walls to undergo yielding and failure stages. Prior to the failure mechanism, all cracks in the concrete and possible yielding of steel in hinging regions have developed. In perforated shear walls, hinging regions are located at both sides of, and between openings, sometimes extending further downward. Thus, diagonal cracks in these hinging regions govern lateral displacement of a wall. These hinging regions are the critical shear zones against lateral load. Solid shear walls potentially have larger maximum displacements than perforated shear walls, when an external load is applied; in that, perforated shear walls have much smaller hinging regions and diagonal cracks. Combining the discussion here and curvature distribution above, the regions below the top of openings are high potential areas for crack development and propagation in perforated shear walls. Therefore, only horizontal steel bars below the top of openings are considered in the establishment of critical loads and displacements of the backbone curve.

8. Effect of diagonal bars

The placement of diagonal steel bars around the openings is an important factor in retaining more strength capacity when subjected to external forces. Observation of displacement from different strain gauges on vertical and diagonal bars shows that the diagonal bar has a large elongation on the tension side, but little compression or tension on the compression side. Lower diagonal bars, which are embedded in the ground on the tension side of openings, are also stressed in tension; while lower diagonal bars on the other side of openings are omitted due to compression. It is concluded that only diagonal bars on the tension side are considered in the computation of the backbone curve.

9. Force at four loading stages

As previously discussed (shown in Fig. 3), backbone curve is composed of four critical stages. Cracking point represents the loading point when initial cracks first appear in the concrete. Yielding point shows the loading stage when the outermost steel bars reach yielding stress. When the applied load cannot be increased, ultimate point is then defined. Beyond this point, the curve shows degrading process. Failure reference point will be defined later.

Some other definitions are to be defined first prior to formulation of the curve. Those are shear span length ratio SSR $(= (M/P)/W$, where M is the moment at the bottom of the wall, P is external load, and W is the width of the wall), height ratio of the opening $\alpha_o(= L_o/L)$, width ratio of opening $\beta_o(= W_o/W)$, horizontal location factor of opening $\beta_1(= W_p/W)$, and vertical location factor of opening $L_{wp}(= L_p/W_p)$. Units shown here are cm, Kg and Kg/cm^2.

Equations of loading capacities at four critical stages are:

9.1 Cracking point

Since initial cracks are solely related to the behavior of concrete, cracking load is defined as

$$P_c = [A_1 + A_2(L_p/L)(\alpha_o \cdot \beta_1)](f_c')^{1/2} \cdot W \cdot t \tag{1}$$

in which

$$A_1 = 0.0212 + 0.2762 \, (SSR) \tag{2}$$

$$A_2 = 1.1531 - 1.2215 \, (SSR) \tag{3}$$

9.2 Yielding point

When the external load reaches yielding point, the behavior of shear walls combines the effects of both steel bars and concrete. The yielding load is then written as

$$P_y = [A_3 + A_4 \cdot \log_{10}[(L_p/L)(\alpha_o \cdot \beta_1)]]P_u \tag{4}$$

in which

$$A_3 = 1.2657 - 0.3188 \, (SSR) \tag{5}$$

$$A_4 = 0.2702 - 0.1362 \, (SSR) \tag{6}$$

9.3 Ultimate point

$$P_u = \tau_u \cdot W \cdot t \tag{7}$$

$$\tau_u = [U_1 + U_2(L_p/L)(\alpha_o \cdot \beta_1)](f_c')^{1/2} + U_3 \cdot PWH + U_4 \cdot PWV \tag{8}$$

PWH and *PWV* calculated at this stage assume all steel bars reach the yielding state. Corresponding effective horizontal and vertical forces, P_h and P_v, used in the formulations will be derived later.

Where

$$U_1 = 0.9320 - 1.1690 \, (SSR) \tag{9}$$

$$U_2 = -1.1741 + 1.5588 \, (SSR) \tag{10}$$

$$U_3 = 0.3128 - 0.3249 \, (SSR) \tag{11}$$

$$U_4 = 0.1759 + 0.3079 \, (SSR) \tag{12}$$

$$PWH = (\Sigma(\rho_{wh} \cdot f_y))(L/W) \tag{13}$$

$$PWV = (\Sigma(\rho_{wv} \cdot f_y))(W/L)^{a_1} \tag{14}$$

in which $a_1 = 4.7663$; ρ_{wh} and ρ_{wv} represent the steel ratios of horizontal and vertical bars, respectively. Derivation of *PWH* and *PWV* is discussed later.

9.4 Failure reference point

P_f is assumed to be half the sum of cracking load and yielding load, which is expressed as

$$P_f = \left(\frac{1}{2}\right)(P_c + P_y) \tag{15}$$

A general notation system defined in Fig. 9 is used for the derivations of *PWH* and *PWV*. Region 1 indicates both sides of the opening, and region 2 the portion below the level of the opening. Both P_h and P_v represent the loads taken by vertical steel bars, horizontal steel bars and diagonal bars in the horizontal and vertical direction, respectively. Three factors, including length reduction, section-area reduction and modification of diagonal bars, are involved in the derivations of P_h and P_v. From Fig. 10, length reduction factor of horizontal bars in region 1 is
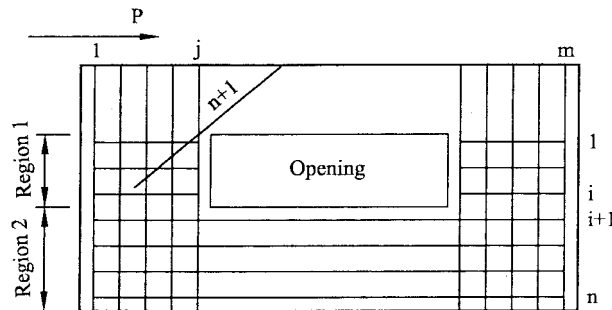

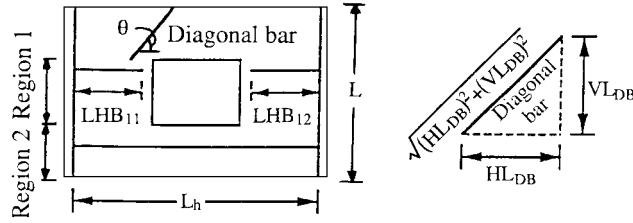Fig. 9 General configuration of steel bars in perforated shear wall

Fig. 10 Length reduction factor for steel bars of perforated shear wall

$$f_{lhh} = (LHB_{11} + LHB_{12})/L_h \tag{16}$$

Length reduction factor of horizontal bars in region 2 is

$$f_{lhh} = L_h/L_h = 1 \tag{17}$$

Length reduction factor for diagonal steel bars in horizontal direction is

$$f_{ldh} = HL_{DB}/L_h \tag{18}$$

and in the vertical direction is

$$f_{ldv} = VL_{DB}/L \tag{19}$$

The projection of a steel bar's normal force in the horizontal and vertical directions, $P(\cos\theta)$ and $P(\sin\theta)$, is formulated as
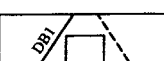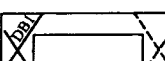
$$P(\cos\theta) = f_y(A_s \cdot \cos\theta) = f_y \cdot A_s \cdot [HL_{DB}/((HL_{DB})^2 + (VL_{DB})^2)^{1/2}] \tag{20}$$

$$P(\sin\theta) = f_y(A_s \cdot \sin\theta) = f_y \cdot A_s \cdot [VL_{DB}/((HL_{DB})^2 + (VL_{DB})^2)^{1/2}] \tag{21}$$

where $HL_{DB}/((HL_{DB})^2 + (VL_{DB})^2)^{1/2} = f_{adh}$ and $VL_{DB}/((HL_{DB})^2 + (VL_{DB})^2)^{1/2} = f_{adv}$ are the cross section area reduction factors of diagonal bars in relation to horizontal and vertical projections, respectively.

As to the modification factor for diagonal bars, the bottom of the diagonal bar, which indicates the lower end not embedded in the ground, is called a semi-rigid point. The diagonal bar has a fixed point, where the lower end embedded in the ground is called the rigid point. Since it is difficult to calculate modification factors for basic development length of diagonal bars, it is assumed to be 0.5 (denoted as f_r) for semi-rigid points and 1.0 for rigid points. Table 2 shows a summary of f_r where NDB denotes the number for effective diagonal steel bars. From Fig. 9, P_h and P_v are

Table 2 Summary of coefficient NDB and f_r

WALL TYPE COEFF.									
NDB	1	2		3			4			
f_r	DB1	DB1	DB2	DB1	DB2	DB3	DB1	DB2	DB3	DB4
	0.5	0.5	1.0	0.5	1.0	1.0	0.5	1.0	0.5	1.0

$$P_h = L \cdot t \left[\sum(\rho_i \cdot (f_y)_i \cdot (f_{lhh})_i)\right] + L \cdot t \left[\sum(\rho_j \cdot (f_y)_j \cdot (f_{adh})_j \cdot (f_{ldh})_j \cdot (f_r)_j)\right]; \quad i = 1, n \text{ and } j = n+1, n+1 \quad (22)$$

$$P_v = \{W \cdot t[\sum(\rho_i \cdot (f_y)_i)] + W \cdot t[\sum(\rho_j \cdot (f_y)_j \cdot (f_{adv})_j \cdot (f_{ldv})_j \cdot (f_r)_j)]\}(W/L)^a;$$

$$i = 1, n \text{ and } j = n+1, n+1 \quad (23)$$

$(W/L)^a$ is a shape factor to adjust critical induced vertical force, P_v, when the horizontal force, P_h, reaches the ultimate state which assumes all effective steel bars, either horizontal or diagonal, attaining the yielding point. Here a is a constant.

Horizontal shear stress τ_h on the horizontal cross section can be defined as $\tau_h = P_h/(W \cdot t)$. Vertical shear stress τ_v can also be defined as $\tau_v = P_v/(L \cdot t)$. Thus,

$$\tau_h = P_h/(W \cdot t) = (L/W)[\sum(\rho_i \cdot (f_y)_i \cdot (f_{lhh})_i)] + (L/W)[\sum(\rho_j \cdot (f_y)_j \cdot (f_{adh})_j \cdot (f_{ldh})_j \cdot (f_r)_j)]$$

$$= [\sum(\rho_{wh} \cdot f_y)](L/W) = PWH; \quad i = 1, n \text{ and } j = n+1, n+1 \quad (24)$$

$$\tau_v = P_v/(L \cdot t) = (W/L)[\sum(\rho_i \cdot (f_y)_i)] + (W/L)[\sum(\rho_j \cdot (f_y)_j \cdot (f_{adv})_j \cdot (f_{ldv})_j \cdot (f_r)_j)](W/L)^a;$$

$$= [\sum(\rho_{wv} \cdot f_y)](W/L)^{a_1} = PWV; \quad i = 1, m \text{ and } j = n+1, n+1 \quad (25)$$

Here from experimental data with curve fitting technique, a_1 in *PWV* is 4.7663.

In Eqs. (13) and (14), $\sum(\rho_{wh} \cdot f_y)$ and $\sum(\rho_{wv} \cdot f_y)$ are defined as

$$\sum(\rho_{wh} \cdot f_y) = (1/(L \cdot t))(EHB) + (1/(L \cdot t))(EDBH) \quad (26)$$

$$\sum(\rho_{wv} \cdot f_y) = (1/(W \cdot t))(EVB) + (1/(W \cdot t))(EDBV) \quad (27)$$

where effect of horizontal bars is

$$EHB = \sum((A_h)_i \cdot (f_y)_i \cdot ((LHB)_i/L_h)) = \sum((A_h)_i \cdot (f_y)_i \cdot (f_{lhh})_i); \quad i = 1, n \quad (28)$$

Effect of diagonal bars in the horizontal direction is

$$EDBH = \sum\{(A_d)_i \cdot (f_y)_i \cdot [(HL_{DB})_i/((HL_{DB})_i^2 + (VL_{DB})_i^2)^{1/2}] \cdot ((HL_{DB})_i/L_h) \cdot (f_r)_i\}$$

$$= \sum((A_d)_i \cdot (f_y)_i \cdot (f_{adh})_i \cdot (f_{ldh})_i \cdot (f_r)_i); \quad i = 1, NDB \quad (29)$$

Effect of vertical bars is

$$EVB = \sum((A_v)_i \cdot (f_y)_i); \quad i = 1, m \quad (30)$$

Effect of diagonal bars in the vertical direction is

$$EDBV = \sum((A_d)_i \cdot (f_y)_i \cdot (f_{adv})_i \cdot (f_{ldv})_i (f_r)_i); \quad i = 1, NDB \quad (31)$$

NDB refers to Table 2. A_h, A_v and A_d denote cross-sectional areas related to horizontal, vertical and diagonal steel bars, respectively.

10. Displacement at four loading stages

Displacements corresponding to the four loading stages are formulated as follows:

10.1 Cracking point

$$D_c = C_D(F_{c1} + F_{c2} + F_{c3})(P_cL/GA_{og})/(f_c'/280)^{1/2} \quad (32)$$

in which

$$C_D = 5.007 - 3.941 \, (SSR) \tag{33}$$

$$F_{c1} = 0.1775 - 9.61(L_p/L)(W_p/W)(\alpha_o \cdot \beta_o) \tag{34}$$

$$F_{c2} = 1903(PWV1) \tag{35}$$

$$F_{c3} = -1092(PWH1) \tag{36}$$

and

$$|F_{c1} + F_{c2}| > |F_{c3}| \tag{37}$$

$$PWH1 = (\Sigma(\rho_{wh}f_y/5000))(L/W) \tag{38}$$

$$PWV1 = (\Sigma(\rho_{wv}f_y/5000))(W/L)^{a_2} \tag{39}$$

$$A_{og} = (W - W_o) \cdot t + \Sigma(n_i - 1)(A_v)_i; \quad i = 1, \, m \tag{40}$$

Here a_2 in $PWV1$ is -0.8418; A_v is the cross sectional area of the vertical steel bar and

$$n_i = E_s/E_c = (f_y/\varepsilon_{sy})/[15000 \cdot (f_c')^{1/2}] = f_y/[37.5 \cdot (f_c')^{1/2}] \tag{41}$$

where E_s and E_c are the moduli of elasticity for steel bars and concrete, respectively. ε_{sy} is assumed to be 0.0025.

10.2 Yielding point

$$D_y = Y_D(F_{y1} + F_{y2} + F_{y3})(P_yL/GA_{og})/(f_c'/280)^{1/2} \tag{42}$$

in which

$$Y_D = -1.878 + 3.773(SSR) \tag{43}$$

$$F_{y1} = 7.697 + 229.2(L_p/L)(W_p/W)(\alpha_o \cdot \beta_o) \tag{44}$$

$$F_{y2} = 2622(PWV1) \tag{45}$$

$$F_{y3} = -6691(PWH1) \tag{46}$$

and
$$|F_{y1} + F_{y2}| > |F_{y3}| \tag{47}$$
Here a_2 in $PWV1$ is 0.6751.

10.3 Ultimate point

$$D_u = U_D(F_{u1} + F_{u2} + F_{u3})(P_uL/GA_{og})/(f_c'/280)^{1/2} \tag{48}$$

in which

$$U_D = -0.7435 + 2.4(SSR) \tag{49}$$

$$F_{u1} = 13.05 + 488.6(L_p/L)(W_p/W)(\alpha_o \cdot \beta_o) \tag{50}$$

$$F_{u2} = 2214(PWV1) \tag{51}$$
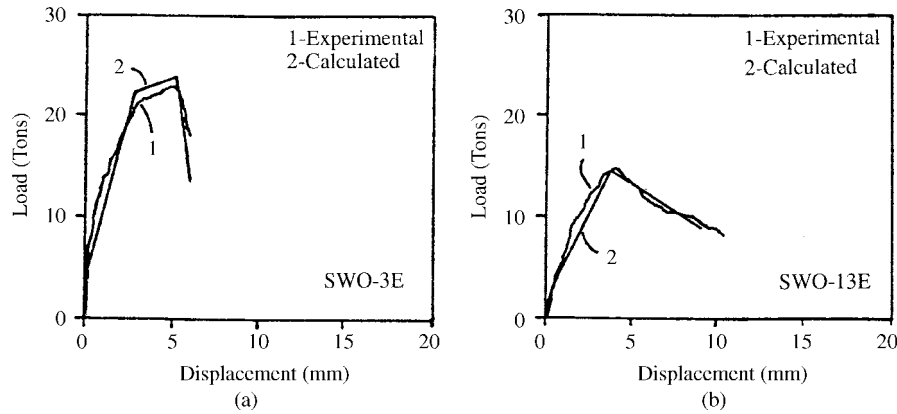
$$F_{u3} = -7685(PWH1) \tag{52}$$

Fig. 11 Comparison between calculated and experimental backbone curves

and

$$|F_{u1} + F_{u2}| > |F_{u3}| \qquad (53)$$

Here a_2 in *PWV*1 is 0.2997.

10.4 Failure reference point

$$D_f = (C_{f1} + C_{f2}(L_{wp}))D_u \qquad (54)$$

in which

$$C_{f1} = 2.2349 - 3.4173(SSR) \qquad (55)$$

$$C_{f2} = 1.5608 - 0.4736(SSR) \qquad (56)$$

11. Comparison of calculated and experimental results

Fig. 11 shows that comparisons between calculated and experimental curves are favorable for shear walls SWO-3E and SWO-13E. The rest of the walls also show good compatibility between computed and experimental results.

12. Conclusions

To investigate the characteristics of isolated low-rise RC perforated shear walls without boundary columns and beams, as well as its load-displacement relationship (backbone curve), a series of tests were conducted. Openings in the test walls include single window, double windows, single slit and single door. Two kinds of walls with height/width ratios of 0.5 and 0.75 are classified. Some solid shear walls were tested for comparison purposes.

From above experimental observations and a theoretical approach, it can be concluded that:

(1) Solid shear walls have much more curvature distribution, load capacity, and lateral displacement than perforated shear walls. Openings in the latter obviously decrease the potential strength capacity and total lateral displacement.

(2) Opening ratios in this paper include 16.35% and 21.8% for walls with height/width ratios of 0.5 and 0.75, respectively. It is not clear that a load-displacement relationship varies with the height/width ratio and opening ratio. Further study will help establish the load-displacement curve in relation to the height/width ratio and opening ratio of the wall.

(3) Bending effects at the bottom of the walls, either from solid or perforated shear walls, contribute larger flexural (bending) displacement than that at the top of the walls.

(4) Comparing bending and shear displacements for both solid and perforated shear walls, it is apparent that shear effect occupies a more important role than bending effect. Shear displacement caused by horizontal steel bars largely increases the potentiality to resist external loads.

(5) Two identified regions exist in perforated shear walls. First, at the top of the wall, there is a wedge-shaped block which provides little influence in strength and lateral displacement. The second, located at both sides of, and between openings, is the hinging region with high interaction of bending and shear, and a determining area to control the failure mechanism of RC shear walls.

(6) Backbone curve (load-displacement relationship) of the low-rise RC perforated shear wall, composed of a set of semi-empirical equations, is expressed by four critical stages. The four critical points include cracking, yielding, ultimate, and failure points; these constitute the total load-displacement relationship. The comparisons between analytical and experimental results are favorable.

Acknowledgements

References

Cheng, F.Y. and Mertz, G.E. (1989), "Inelastic seismic response of reinforced concrete low-rise shear walls and building structures", NSF Report, NTIS No. PB90-123217. U.S. Department of Commerce. Washington, D.C.

Cheng, F.Y., Ger, J.F., Mertz, G.E. and Sheu, M.S. (1993), "Computed versus observed inelastic seismic low-rise RC shear walls", *J. Struct. Eng*., ASCE., **119**(11), 3255-3275.

Chiba, O., Fukuzawa, R., Hatori, T. and Yagishita, K. (1985), "Experimental study on heavily reinforced concrete shear walls", *Trans. 8th SMiRT Conf.* H 4/1. 131-136.

Higashiura, A., Kubo, T., Sato, K., Sato, Y. and Yamanouchi, H. (1987), "Load-deflection characteristics of shear walls with openings", *Proc. 9th Int. Conf. on Structural Mechanics in Reactor Technology*, Lausanne. **H**, 537-542.

Katagihara, K., Kawamura, H. and Yamada, M. (1974), "Reinforced concrete shear walls with openings; test and analysis", *Shear in Reinforced Concrete*. **2**(SP-42), ACI, Detroit, 559-578.

Korenaga, T., Murazumi, Y., Sotomura, K. and Yoshizaki, S. (1985), "Ultimate shear strength of shear wall in nuclear power plant", *Trans. 8th SMiRT Conf*., H4/4, 145-150.

Sheu, M.S. (1988), "Behavior of low rise RC shear walls subjected to reversed cyclic loading", Technical Report to the National Science Council, Architectural Engineering Department, National Cheng Kung University.